

Robust Biobased Membrane: Self-Entangled Cellulose Nanofibrils–ZnO–Ag Composite with High Photocatalytic Performance for Efficient Dye-Contaminated Water Treatment

Jungsoo Han, Ngoc Bao Tri Pham, Kyudeok Oh, and Han-Kyu Choi*



Cite This: *ACS Omega* 2024, 9, 7143–7153



Read Online

ACCESS |

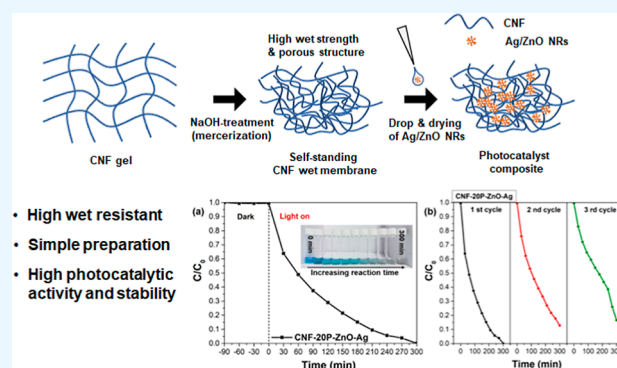
Metrics & More

Article Recommendations

Supporting Information

ABSTRACT: This study presents a simple and effective method for fabricating a porous photocatalyst composite membrane with excellent wet strength, utilizing cellulose nanofibril (CNF) and zinc oxide–silver (ZnO–Ag) nanorod (NRs) for treating dye-contaminated water. The self-standing CNF membrane with a high wet strength was prepared by NaOH treatment. Besides wet strength, NaOH treatment also controlled the pore characteristics of the CNF membrane, which could tightly attach NRs in them. The photocatalyst composite was prepared by simply drop-drying ZnO–Ag NRs onto the CNF membrane, ensuring attachment within the pores. The photocatalytic activity of the composite was evaluated for the degradation of the methylene blue dye under visible light. Despite the straightforward drop-drying method used to cast the ZnO–Ag NRs

onto the CNF membrane, the NRs were not washed out when in contact with water, resulting in a composite that exhibited both high photocatalytic activity and high wet strength. This exceptional performance can be attributed to the tight attachment of the photocatalytic ZnO–Ag NRs to the porous structure of the CNF. Furthermore, the composite demonstrated satisfactory reusability, as no significant deterioration in the photocatalytic performance was observed even after being reused for three cycles. Given its simple preparation method, impressive photocatalytic performance, and durability, we expect that our composite will hold significant value for practical applications in wastewater treatment.



- High wet resistant
- Simple preparation
- High photocatalytic activity and stability

INTRODUCTION

Discharged dye-contaminated water from various industries, such as textiles, paper, and leather, results in significant water pollution, which can have detrimental effects on ecosystems and human health. Photocatalytic inorganic materials have attracted great attention as potential solutions for treating dye-contaminated water.¹ This simple and ecofriendly process involves the use of light to activate transition metals like titanium dioxide and zinc oxide (ZnO), which generate reactive oxygen species (ROS). These ROS then degrade organic compounds such as dyes in contaminated water. ZnO is a well-known photocatalyst candidate for photodegrading dye-contaminated water^{2–5} due to its high activity, strong oxidation ability,⁶ low cost, and nontoxic features.⁷ However, the pure form of ZnO exhibits slow photodegradation due to the high recombination rate of charge carriers within the material.^{8,9} To address this issue, silver nanoparticles (AgNPs) have been employed as a support for ZnO, leading to a significant enhancement in the photocatalytic efficiency of ZnO. This enhancement is attributed to the localized surface plasmon resonance (LSPR) of AgNPs, which can facilitate charge transport⁷ and enhance the separation of charge carriers¹⁰ within metallic oxide semiconductors like ZnO,

titanium dioxide, copper(II) oxide, and tungsten trioxide. Consequently, ZnO nanorods (NRs) decorated with AgNPs achieve 100% dye degradation after 3 h of visible irradiation,⁷ whereas pure ZnO NRs can only achieve 14% degradation within the same time period. Thus, AgNPs-decorated ZnO nanomaterials have become a popular choice for photocatalytic applications.^{9,11,12} However, the typical powder form of ZnO photocatalyst can lead to secondary pollution after the photocatalysis process.¹³ Moreover, the recovery of the catalyst after dye degradation for reuse can also be challenging due to its water-dispersible powder form, limiting its practical applications.

One potential solution to overcome these challenges is to use a platform material with a large size to accommodate small photocatalytic particles such as NRs and nanospheres, thereby creating a photocatalyst composite. Among various options,

Received: November 14, 2023

Revised: January 15, 2024

Accepted: January 19, 2024

Published: January 30, 2024



cellulose stands out as a suitable candidate for this platform material due to its biodegradability, sustainability, abundance, and insolubility in water, making it usable in water-based applications. Among the various types of cellulose materials, cellulose nanofibril (CNF) has been extensively studied for preparing photocatalyst composites. CNF refers to nanoscale cellulose fibril, typically produced by mechanical fibrillation of cellulosic raw materials such as wood pulp and cotton.¹⁴ Due to its high aspect ratio and nanoscale dimension, CNF possesses a large specific surface area, enabling effective attachment of metal NPs through direct synthesis.¹⁵

In practical applications, it is essential to establish strong bonding between the photocatalytic particles and the cellulose substrate to prevent the release of the particles in water and subsequent secondary pollution. Until now, the composite has usually been prepared by direct synthesis of metal NPs on the cellulose substrate^{16–20} and utilization of post-treatments such as microwave and hydrothermal treatment to precisely control the size and shape of the nanoparticles.^{16,18,20} However, these post-treatments, involving a high temperature and pressure in the presence of water, can disrupt the hydrogen bonding between cellulose fibers and weaken the structure of the composite. The strength of cellulose-based materials, such as paper and membranes, largely relies on the hydrogen bonding between the cellulose fibers. Consequently, they are unsuitable for photocatalyst applications without additional treatments to develop wet strength, as they can easily break down when exposed to running water. As a result, most research on photocatalyst composites based on cellulose substrates has focused on fiber materials such as CNF, rather than the structured materials such as paper or membrane. However, compared to larger materials like paper, the one-dimensional photocatalyst composite based on fiber materials is inconvenient in terms of collection and reuse.

In this study, we demonstrate the straightforward approach to prepare a photocatalyst composite membrane based on a CNF. AgNPs-decorated ZnO NRs (ZnO–Ag) were synthesized through the hydrothermal method and used as the photocatalyst. In addition, the self-standing CNF membrane with high wet strength was prepared by immersing the wet CNF cake in a NaOH solution. By combining the self-entanglement behavior of the CNF during the NaOH treatment and the use of CNFs of varying widths, we can control the pore size of the CNF membrane. For preparing the photocatalyst composite, we simply dropped the ZnO–Ag NRs solution onto the membrane and allowed it to dry. Interestingly, the ZnO–Ag NRs were tightly embedded within the membrane, possibly due to their attachment to the pores of the membrane. This composite membrane exhibits exceptional photocatalytic performance in the degradation of methylene blue (MB) dye under visible light. Remarkably, even after 5 h of light irradiation, the composite achieves complete degradation of the dye. Importantly, we observe no significant deterioration in the photocatalytic performance of the composite membrane, even after it is reused for three cycles. Our findings highlight the favorable reusability and photocatalytic efficiency of the composite membrane, underscoring its potential for practical applications in the field of photocatalysis.

EXPERIMENTAL SECTION

Materials. Hardwood bleached kraft pulp (HwBKP, a mixture of aspen and poplar from Canada) was kindly

provided from a paper mill in Korea for the purpose of preparing CNF. Zinc acetate dihydrate ($\text{Zn}(\text{CH}_3\text{COO})_2 \cdot 2\text{H}_2\text{O}$, 99.999%) was purchased from Sigma-Aldrich (USA). Sodium hydroxide (NaOH), silver nitrate (AgNO_3), MB trihydrate ($\text{C}_{16}\text{H}_{18}\text{N}_3\text{SCL} \cdot 3\text{H}_2\text{O}$), and phenol ($\text{C}_6\text{H}_5\text{OH}$) were purchased from Samchun Chemicals (Korea) and used without purification.

Preparation of CNF. HwBKP suspension with 2 wt % consistency was disintegrated using a laboratory valley beater, and then it was repeatedly ground by passing through a super masscolloider (SMC; MKGA-6, Masuko Corp., Japan) at 1500 rpm. The gap between the two grinding stones of SMC was set to $-120 \mu\text{m}$ from the zero position by controlling the bottom grinding stone after HwBKP was loaded. We produced CNFs with different dimensions by varying the number of passes through the SMC. CNFs were collected after 10, 20, and 30 passes through the SMC, and each CNF was denoted as CNF-10P, CNF-20P, and CNF-30P, respectively.

Preparation of Self-Entangled CNF Membrane. The CNF suspension was diluted to a concentration of 0.2 wt % in water using an Ultra Turrax instrument (T-25, IKA, Germany) at 12,000 rpm for 10 min and degassed. The desired amount of CNF suspension was then subjected to vacuum filtration on a cellulose acetate membrane ($0.45 \mu\text{m}$ pore size, HYUNDAI MICRO, Republic of Korea) with a target basis weight of $50 \text{ g}/\text{m}^2$. The obtained wet CNF cake with the membrane was immersed in 20 wt % NaOH (aq) solution and kept at $50 \text{ }^\circ\text{C}$. During this process, the self-entangled membrane sheet, which was able to be handled separately from the membrane, was formed. After a 30 min treatment with NaOH solution, the CNF membrane was subsequently transferred to a bath containing a 2 wt % acetic acid (aq) solution and kept for 30 min for a neutralization. Finally, the neutralized CNF membrane was thoroughly rinsed under running water overnight. The prepared CNF membrane was frozen in liquid nitrogen and lyophilized using a freezing dryer (FD8508, Ilshin Lab. Co., Ltd., Korea).

Preparation of ZnO NRs and ZnO–Ag NRs. The ZnO and ZnO–Ag NR samples were prepared through the hydrothermal method as reported by Wei et al.²¹ The solution of $\text{Zn}(\text{CH}_3\text{COO})_2 \cdot 2\text{H}_2\text{O}$ (0.059 M, 32 mL) was mixed with NaOH solution (4 M, 4 mL). Then, 10 mL of AgNO_3 (0–5 wt %) was added into the mixture under continuous stirring for 10 min to obtain the reaction solution system. The uniform solution was transferred into a Teflon-line autoclave and heated at $180 \text{ }^\circ\text{C}$ for 12 h. Then, the final product was centrifuged with deionized (DI) water and ethanol multiple times and dried in an oven at $65 \text{ }^\circ\text{C}$. At last, the prepared sample was collected in powder form. For pure ZnO, the process was the same as mentioned above, without AgNO_3 .

Preparation of CNF–ZnO–Ag and CNF–ZnO composites. The CNF membrane with NaOH treatment was cut into small pieces ($1 \times 1 \text{ cm}$) for the preparation of composites. It was dried in an oven at $65 \text{ }^\circ\text{C}$ for 2 h to reduce the humidity of the membrane. After that, the CNF sample was heated on the hot plate at $80 \text{ }^\circ\text{C}$, and 2 mL of ZnO–Ag or ZnO NRs (2.20 wt % in EtOH) was drop-cast on both sides of the surfaces of the CNF sample. After that, the composite membrane could be used for a photocatalyst experiment.

Characterization of CNF. The tensile strength of the wet membrane was measured by using a tensile tester (STB-1225S, AND, Japan) equipped with a 2.5 kN load cell. Specimens of $5 \text{ mm} \times 35 \text{ mm}$ in size were prepared, and the length of the test

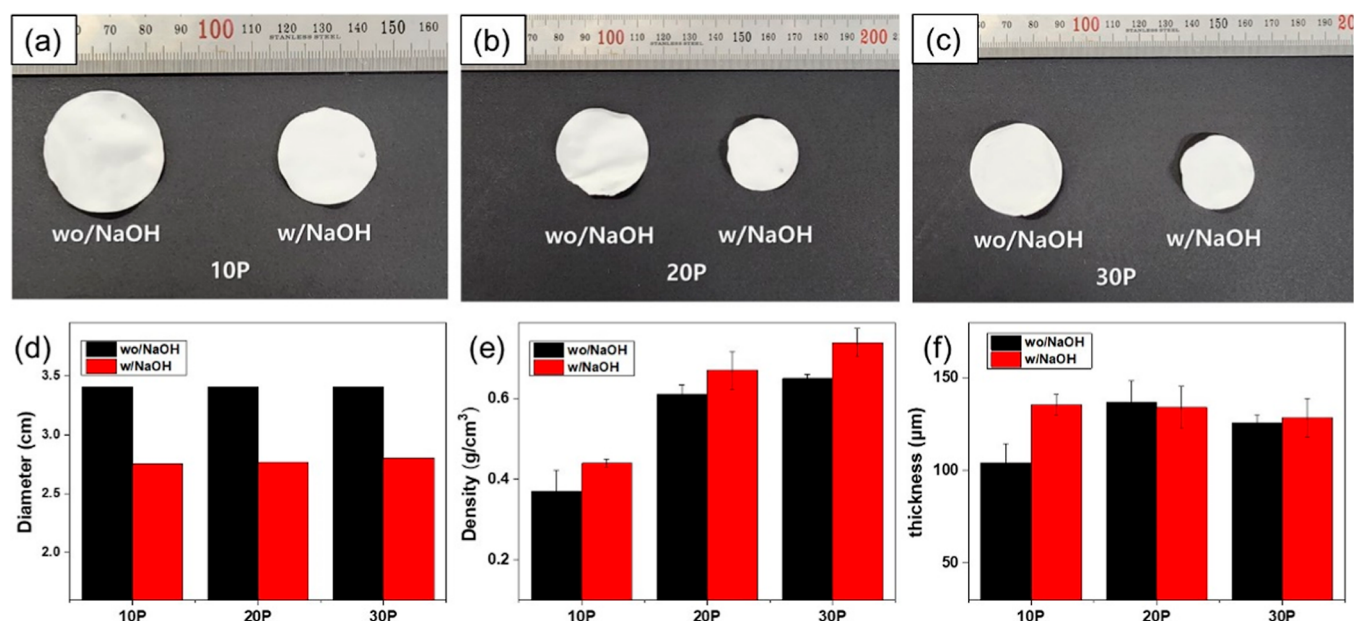


Figure 1. Photographs and dimensional change results of CNF sheets by NaOH treatment. (a–c) Photographs of CNF sheets with different degrees of fibrillation without or with NaOH treatment. Dimensional change of CNF membranes: (d) diameter, (e) thickness, and (f) density (Photograph courtesy of J. Han. Copyright 2023).

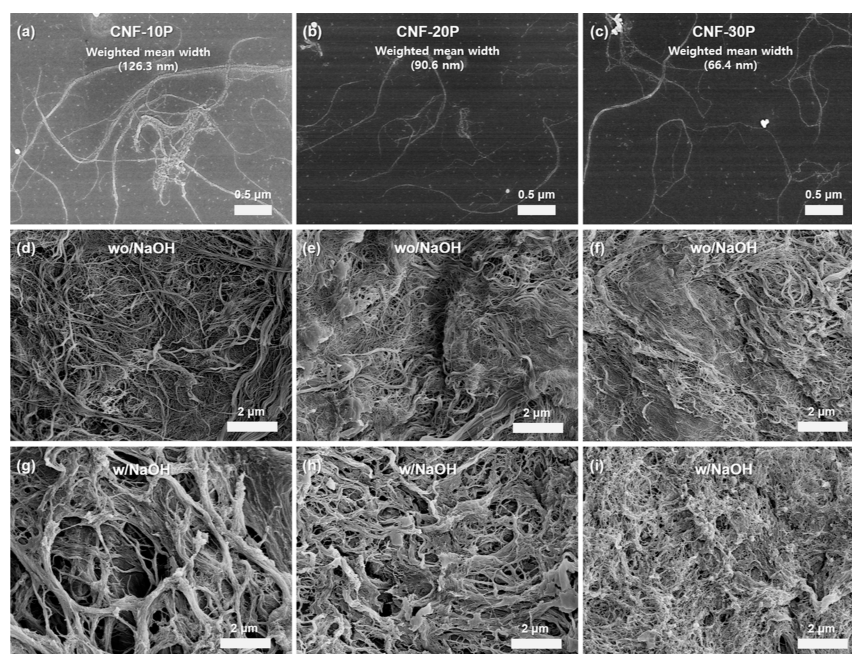


Figure 2. SEM images of the prepared CNFs and their sheets without or with NaOH treatment. (a–c) Prepared CNFs with different degrees of fibrillation. (d–f) CNF sheets without NaOH treatment (wo/NaOH). (g–i) CNF sheets with NaOH treatment (w/NaOH).

span was set at 25 mm. Before testing, the water on the specimen surface was carefully wiped out using a filter paper. The tensile test was conducted at a crosshead displacement speed of 1 mm/min at 23 °C and 50% relative humidity. The thickness of each sample was measured using a digital micrometer (Digimatic 293-521-30, Mitutoyo, Japan), and the density (g/cm³) of each film was calculated from the basis weight (g/m²) divided by the thickness (μm). The wet membrane was freeze-dried for other characterizations.

The X-ray diffraction (XRD) patterns of samples were obtained using an X-ray diffractometer (D8 DISCOVER, Bruker AXS, Germany) equipped with a Cu K α radiation

source, operating at 40 kV, 40 mA, $2\theta = 5\text{--}50^\circ$, a divergence angle of 0.2° , and a step size of 0.02. Attenuated total reflectance–Fourier transform infrared spectroscopy (ATR–FTIR) was performed to characterize the chemical structure of samples. FTIR spectra were recorded on a Nicolet Nexus 670 instrument equipped with a KRS-5 crystal of refractive index 2.4, using an incidence angle of 45° . The spectra were collected in a transmittance mode within the wavenumber range of $400\text{--}4000\text{ cm}^{-1}$, with a resolution of 4 cm^{-1} and an accumulation of 128 scans.

Mercury intrusion porosimetry measurements were conducted on freeze-dried membranes by using a mercury

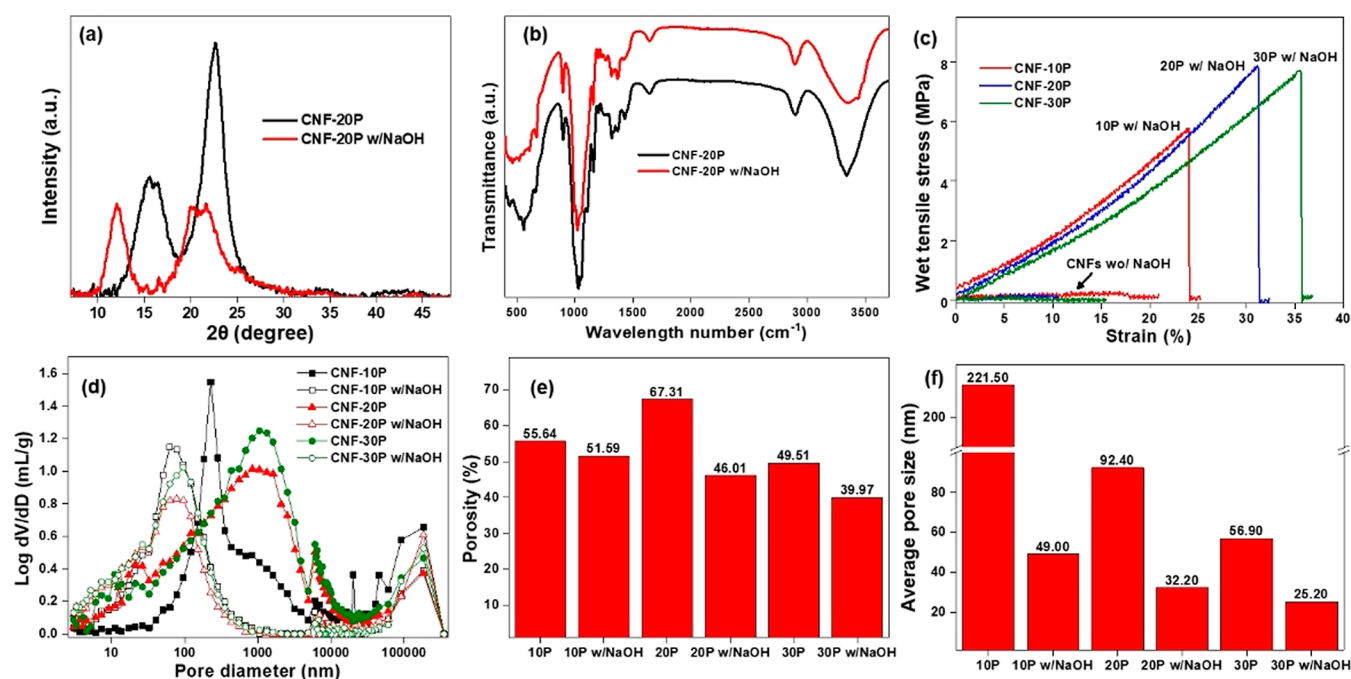


Figure 3. Characteristics of prepared CNF membranes without (w/NaOH) and with NaOH treatment (w/NaOH). (a) XRD patterns, (b) ATR-IR spectra, (c) stress–strain curve, (d) pore size distribution, (e) average pore size, and (f) porosity. (d–f) Are determined by mercury porosimetry.

porosimeter (Autopore IV 9520, Micrometrics, UK). The morphologies of the CNF, membrane, ZnO–Ag NRs, and composite were analyzed by [field emission scanning electron microscopy (FE-SEM) (S-4800, Hitachi, Japan). For measuring the widths of CNFs, a droplet of 0.01 w/v % of the diluted CNF/water suspension was deposited on a silicon wafer and air-dried. The dried wafer sample was coated with a platinum layer and observed with FE-SEM at an accelerating voltage of 5–10 kV. The widths of the CNFs were evaluated at identical magnifications using the image analysis program. The measured width for each sample was at least 300.

Photocatalytic Experiment. The photocatalytic performance of samples was determined by the photodegradation of MB aqueous solution under visible light (solar simulator, 66902, Newport; equipped with a 300 W Xe arc lamp and a 420 nm long pass filter) at room temperature. The sample (1 × 1 cm) with a weight of approximately 0.04 g was placed in 200 mL of a 10 mg/L MB solution. Prior to light irradiation, the suspension was mechanically agitated in the dark for 90 min under magnetic stirring conditions to establish an adsorption/desorption equilibrium between MB and sample. The MB solution was collected at regular time intervals (30 min under dark conditions and 15 min under light irradiation conditions) to evaluate the photocatalytic activity. The concentration of MB was determined by recording its absorbance at 664 nm wavelength using a UV–vis spectrometer (UV-2600i, Shimadzu). The degradation efficiency was then calculated based on the absorbance data.

RESULTS AND DISCUSSION

Characteristics of CNF Membranes. We measured the weights and apparent dimensions of the CNF membrane both with and without NaOH treatment after freeze-drying. Through NaOH treatment, the weight of the membrane was reduced by approximately 15.08 ± 0.9 wt %. It was attributed

to the dissolution of hemicellulose in the CNF from the wood fiber.²² Additionally, the membranes exhibited a decrease in width in a wide direction (Figure 1a–d) and an increase in thickness (Figure 1e). The dimensional change rates of CNF membranes were higher for the diameter compared with the thickness (Figure 1d,e). Consequently, the density of the membranes increased after NaOH treatment (Figure 1f). The NaOH treatment led to immediate aggregation and entanglement of CNFs within the membrane, resulting in a significant dimensional change.

To characterize the morphologies of CNFs with different SMC pass numbers as well as the membrane structures before and after NaOH treatment, FE-SEM analysis was performed (Figure 2). With an increasing number of fibrillation passes, the width of the CNFs decreased and the fibril aggregates disappeared (Figure 2a–c). The weighted mean values of the width of CNFs ranged from 126.3 to 66.4 nm, based on each CNF width measurement. As the CNF width decreased, the prepared membrane exhibited a more densely packed fibril network and a smaller pore distribution (Figure 2d–f). Upon NaOH treatment, however, the structure of CNF membranes underwent significant transformation (Figure 2d,g, 2e,h, and 2f,i, respectively). The surface of CNF membranes treated with NaOH solution showed the formation of larger fibril bundles with kinky features, which are attributed to the twist of each CNFs and the aggregation of neighboring CNFs caused by NaOH treatment.²³ Cellulose naturally contains both highly ordered (crystalline) and less ordered (amorphous) structures. Cellulose derived from natural plants, including wood, possesses a crystalline structure called cellulose I, where cellulose chains are tightly packed in parallel arrays. In the process of immersing cellulose in a NaOH solution and subsequent washing to eliminate NaOH, the crystalline structure undergoes a transformation in polarity. The initial parallel arrays configuration of cellulose changes to antiparallel

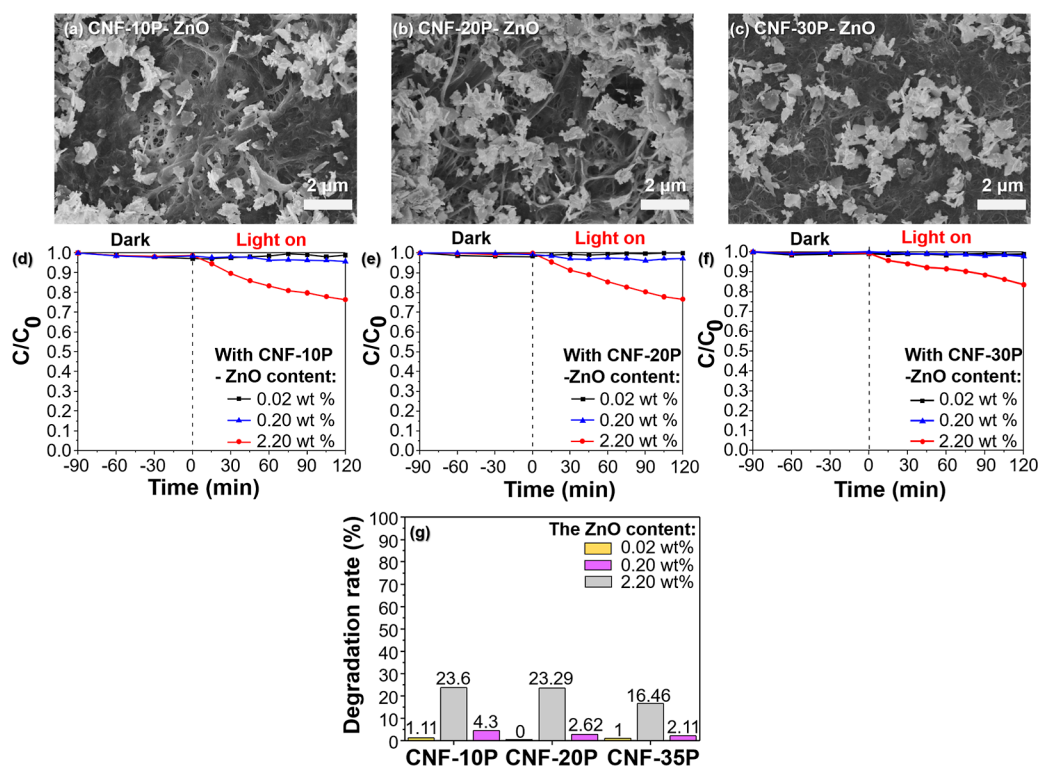


Figure 4. (a–c) SEM images of the CNF–ZnO composite with the three types of CNF and content of ZnO (2.20 wt %). (d–f) Photocatalytic effect of the CNF–ZnO composite with the three types of CNF and varied content of ZnO. (g) Degradation bar chart of MB in the presence of CNF–ZnO with variations of ZnO content and CNF type.

arrays, commonly referred to as cellulose II.²⁴ When cellulose is immersed in NaOH solution, NaOH hydrate molecules penetrate the amorphous structure and diffuse into the cross sections, enabling individual cellulose chains to fold back on themselves to form antiparallel arrays of cellulose II.²⁵ These conformational changes in cellulose chains during NaOH treatment contribute to the morphological changes in CNFs (Figure 2).^{26,27} These morphological changes of CNFs occur largely in the NaOH solution with a concentration over 15 wt %, which would lead to a strong entanglement of CNFs in the membrane.²³ That is why we use the 20 wt % NaOH solution to make the CNF membrane.

The entanglement of CNFs within the membrane occurs as a result of the morphological changes induced by NaOH treatment, leading to the formation of a strong woven network. This strong woven network is crucial in making the CNF–ZnO–Ag composite resistant to breakage upon exposure to water, which is important for preventing secondary pollution by the leakage of photocatalyst NRs from the composite. In the NaOH-treated sample, the width of the aggregates formed and the pore sizes in the CNF sheets decreased as the pass number increased. Particularly, in the CNF–30P sheet treated with NaOH (Figure 2i), a remarkable change in the width of CNF aggregates and pore structure was observed.

The self-entanglement of CNFs in the membrane by the NaOH treatment can be attributed to the crystalline structural change in cellulose consisting of CNFs. The XRD pattern of the membrane before and after NaOH treatment indicates a transformation from the cellulose I crystal structure [14.8° and 22.8° for (1–10) and (200) planes, respectively] to cellulose II [12.3°, 20.5°, and 21.9° for (1–10), (110), and (020) planes, respectively]. The change in the crystalline structure from

cellulose I to cellulose II is also evident in the ATR–FTIR spectrum, specifically in the hydroxyl group stretching vibration (–CH–OH and –CH₂–OH) at 3300–3400 cm^{–1}, which corresponds to the inter- and intramolecular hydrogen bonds between cellulose chains. NaOH treatment leads to a broadening of this peak, indicating the disruption of intermolecular hydrogen bonds and the formation of new intramolecular hydrogen bonds as a result of the crystalline structural change. Additional signature bands of cellulose II, such as C–O vibration at 1060–1070 cm^{–1}, antisymmetric in-phase ring stretching vibration at 1110 cm^{–1}, and symmetrical CH vibration at 1440 cm^{–1}, are also observed.^{28,29} Figure 3c shows the mechanical properties of CNF membranes in the wet state. In the absence of NaOH treatment, CNFs in the membrane fail to form hydrogen bonds, leading to a low wet strength (wo/NaOH in Figure 3c). However, the entanglement of CNFs induced by NaOH treatment significantly enhances the wet strength of the membrane (CNFs w/NaOH, Figure 3c). Increasing the pass numbers during CNF production reduces the dimensions of CNFs, resulting in higher tensile stress and strain of the membrane. This effect can be attributed to the increased specific surface area of CNFs, which improves their ability to undergo self-entanglement through NaOH treatment. The enhanced wet strength of the CNF-based photocatalyst composite prevents easy breakage during application in the running water. Mercury porosimetry analysis was performed on the membranes, and the results are presented in Figure 3d–f. As the width of CNF decreases, the porosity and average pore size of CNF-10P, CNF-20P, and CNF-30P are determined as follows: 55.6% and 221.5 nm, 67.3% and 92.4 nm, and 49.5% and 56.9 nm, respectively. Notably, CNF-10P exhibits a different pore size

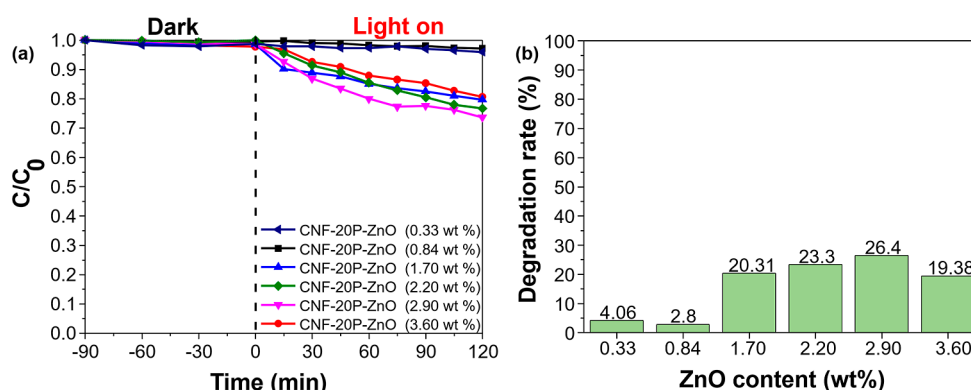


Figure 5. (a,b) Plot of C_t/C_0 versus time and the degradation bar chart of MB in the presence of CNF–ZnO with the variation of the ZnO content.

distribution compared with the other CNFs. By NaOH treatment, the pore size and porosity of CNFs remarkably decreased. The porosity of CNFs changes to 51.5, 46.0, and 39.9%, respectively (Figure 3e). The porosity of CNF-10P was less changed after NaOH treatment compared to that of the other CNFs, which is attributed to the limited development of self-entanglement of CNF-10P due to its larger dimension. Furthermore, NaOH treatment leads to a dramatic shrinkage in the average pore diameter of CNF-10P, CNF-20P, and CNF-30P, which become 49.0, 32.0, and 25.2 nm, respectively (Figure 3f). The remarkable decrease in the pore size of CNF-10P, rather than its porosity change, is attributed to its heterogeneous pore distribution.

Photocatalytic Performance of the CNF–ZnO–Ag Composite. *Effect of CNF Type.* To fabricate the photocatalyst composite, we employed the drop-cast method to attach the photocatalyst to the CNF sheet. Initially, CNF–ZnO composites with different CNF samples were prepared by drop-casting the ZnO NRs onto NaOH-treated CNF membranes, and their photocatalytic performances were evaluated. The attachment of the photocatalyst, including AgNPs and ZnO NRs, to the CNF sheet is crucial to prevent subsequent secondary pollution when the composite is utilized in water. The attachment ability of the CNF sheet is dependent on its pore size. In the composite prepared using CNF-10P (Figure 4a), large agglomerates of ZnO particles were observed within the pores. CNF-10P possessed the largest pore size (Figure 3f), which facilitated excessive agglomeration of ZnO NRs onto the porous matrix, leading to accelerated recombination of holes and electrons,^{30,31} thereby negatively impacting the photocatalytic reaction. In contrast, the composite prepared using CNF-20P, with a smaller pore size and lower porosity, exhibited an even distribution of small nanocatalyst particles around the pores, resulting in improved photocatalytic activity compared to that of the other two membranes (Figure 4b,e). On the other hand, CNF-30P, with its smallest pore size and lowest porosity, had a lower loading of ZnO NRs and experienced severe agglomeration of the nanocatalyst particles (Figure 4c). Consequently, CNF-30P failed to enhance the photocatalytic capability of the composite membrane as these factors hindered the efficient photocatalytic performance. Note that the ZnO–Ag NRs also exhibited good attachment to the CNF sheet (Figure S1 in Supporting Information-A).

The photocatalytic performances of the composites can be attributed to the distinct pore structure and morphology of the CNF membranes (Figure 2), which can affect the strength of

photocatalyst attachment in the CNF membrane. This finding is essential for considering the influence of CNF when evaluating the photocatalytic effect of the composite membrane. Furthermore, although CNF itself does not exhibit photocatalytic activity, its supportive role in the composite membranes is crucial for the overall activity of the membranes. In some cases, cellulose can impede light absorption, prevent electron generation, and diminish the degradation effect of composite.³² However, in most cases, cellulose with a porous structure possesses a high surface area and can provide more active sites, thereby increasing the surface adsorption of reaction species on the surface of the catalyst, which favors the enhancement of photocatalytic performance.³³

Figure 4d–f indicates that CNF-20P exhibited the most optimal type of CNF for the preparation of composite membranes. CNF-10P, containing a low concentration of ZnO (0.02 wt %), exhibited unstable behavior with oscillations during the degradation of MB under light irradiation (the black line in Figure 4d). In contrast, the stable composites (black lines in Figure 4e,f) did not display such oscillations. This instability observed in CNF-10P could potentially impact its subsequent photocatalytic activity. On the other hand, CNF-30P, with a high concentration of ZnO (2.20 wt %), showed low photocatalytic activity (the red line in Figure 4f). The degradation efficiencies of CNF-10P and CNF-20P are quite similar, while CNF-30P exhibited slower efficiency (Figure 4g). As observed from all of these findings, CNF-20P is the optimized sample in our experiment.

Effect of the ZnO Content on CNF. To optimize the photocatalytic performance depending on the concentration of ZnO NRs, we prepared ZnO NRs with varying relative contents of ZnO and drop-dried them on CNF-20P (Figure 5a,b). It was determined that a ZnO content of 2.20 wt % was suitable for the fabrication of the composite membrane, as it exhibited excellent photocatalytic performance without ZnO being washed out from the CNF membrane. Increasing the ZnO content to 2.90 wt % induced the photodegradation effect, but an excessive amount of catalyst led to ZnO being leached out from the CNF membrane in an aqueous solution, causing secondary pollution. Figure S2 and Table S1 in Supporting Information-B indicate that some ZnO leaked out of the CNF membrane and dispersed in the DI water for ZnO contents of 2.90 and 3.60 wt %. Furthermore, the photocatalytic rate dramatically declined for the highest ZnO content (3.60 wt %) on CNF, which can be attributed to the significant leakage of ZnO from the CNF membrane.

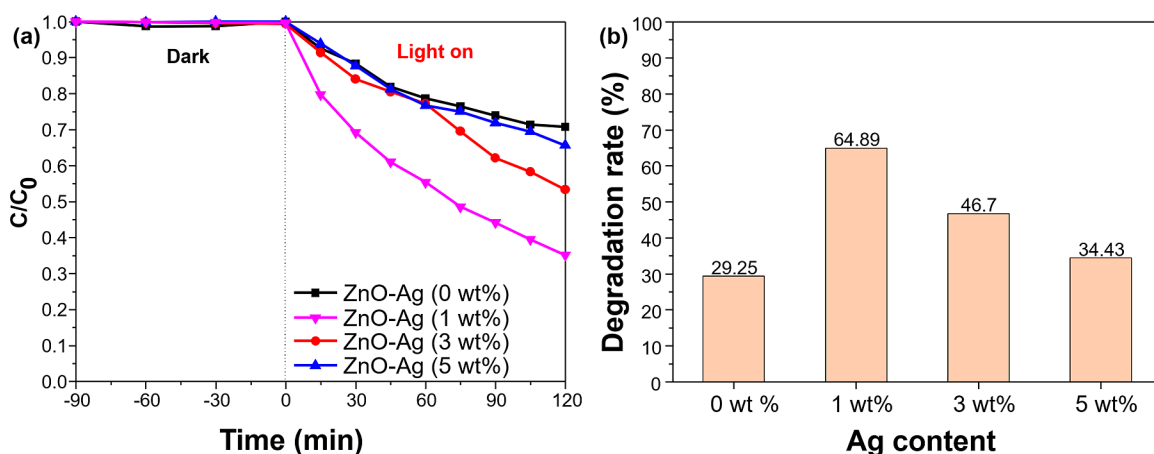


Figure 6. (a,b) Plot of C_t/C_0 versus time and the degradation bar chart of MB in the presence of ZnO–Ag with variations of the silver content.

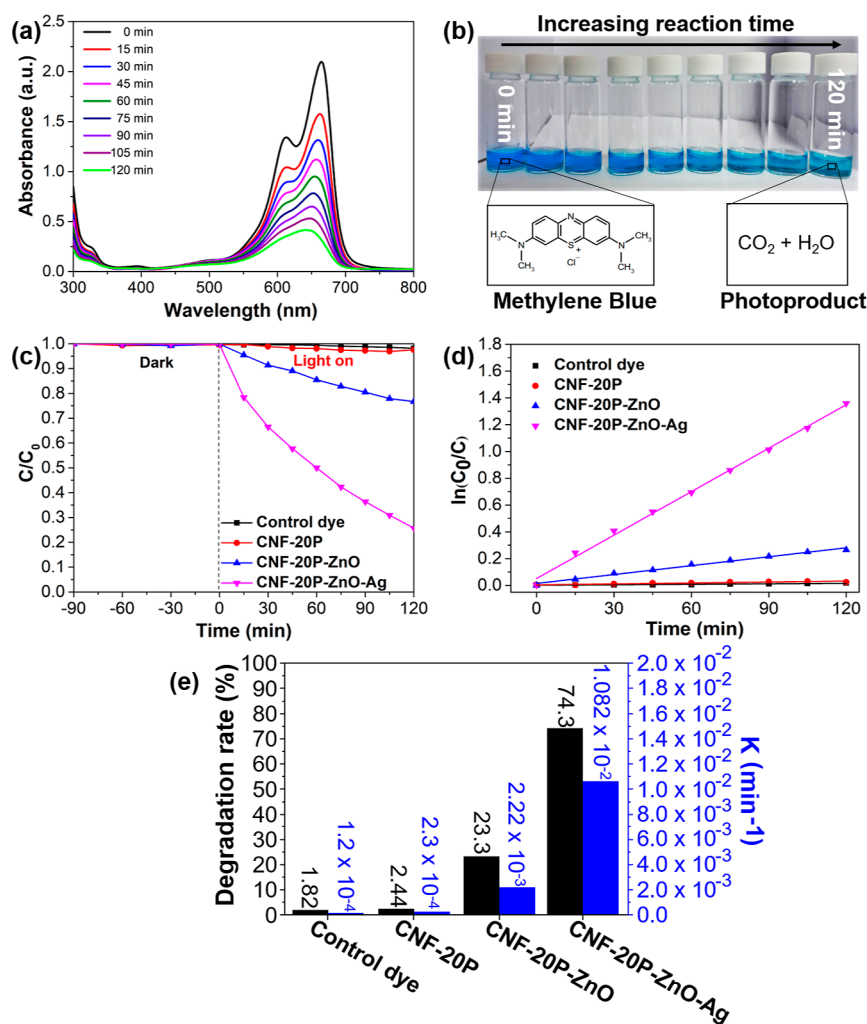


Figure 7. (a) UV–vis spectra of the MB solution in the presence of the CNF–ZnO–Ag composite. (b) Visual image of the degraded product at different times of irradiation. (c) Photocatalytic degradation rate and (d) photocatalysis kinetics of MB over the different samples under visible light irradiation. (e) Histogram of the degradation parameter of MB by various samples. (Photograph courtesy of N. B. T. Pham. Copyright 2023.).

Effect of the Amount of AgNPs Decorated on ZnO NRs. In an effort to enhance the photocatalytic performance of ZnO NRs, we explored the decoration of AgNPs on the surface of ZnO NRs. The silver content was increased to promote the deposition of AgNPs on the ZnO NRs surface. Surprisingly, the optimum ZnO–Ag NRs content for the preparation of

CNF–ZnO–Ag membrane was found to be only 1 wt % (Figure 6a,b), due to a reported light-shielding effect. The high density of AgNPs covering ZnO NRs can rapidly deteriorate the photocatalytic performance of the heterostructure by preventing the interactions between ZnO NRs, light, and organic pollutant molecules.⁷ To further investigate the

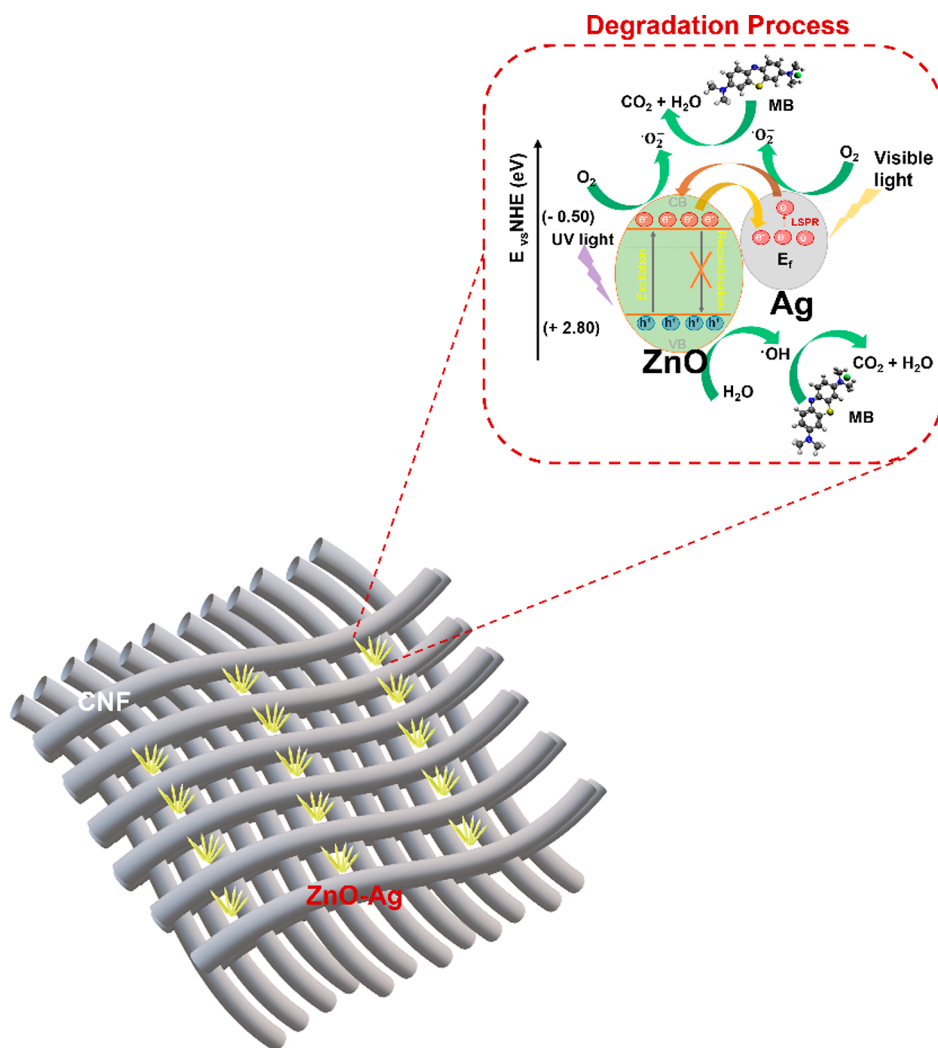


Figure 8. Photodegradation mechanism of the CNF–ZnO–Ag composite.

crystalline structure of the ZnO–Ag NRs in the composite, ZnO–Ag (1 wt %) and ZnO were subjected to XRD analysis (Figure S3 in Supporting Information-C). These prominent peaks in the 30–80° range corresponded to the wurtzite phase of ZnO.³⁴ In addition, the strong peak at approximately 38.39, 44.62, and 64.95° represented the (111), (200), and (220) crystal planes of cubic silver.³⁵ The morphology of the as-prepared ZnO exhibits a NR shape, which aggregates to form a nanoflower-like structure, with average lengths and diameters of approximately 496.34 ± 144.52 and 121.50 ± 38.72 nm, respectively (Figure S4a in Supporting Information-D). In the case of ZnO–Ag, Ag NPs were decorated on the ends of the ZnO NRs, with an average diameter of approximately 33.9 ± 8.2 nm (Figure S4b in the Supporting Information-E). Additionally, Ag NPs with a diameter of 74 nm were also prepared for a comparative photocatalytic experiment (Figure S5a in the Supporting Information-E). Despite Ag NPs being recognized for their high photocatalytic performance without the presence of any semiconductor material,^{36,37} in this study, Ag NPs exhibited no photocatalytic effect on MB within the same period of time as ZnO–Ag (Figure S5b in Supporting Information-E). To compare the degradation effect between ZnO NRs and another ZnO nanostructure, namely, nanosheets (NSs), ZnO NSs were prepared following the precipitate method. The morphology of the as-prepared ZnO NSs exhibits

a NS shape with an average size of 94.65 ± 49.12 nm and an average thickness of 15.92 ± 3.70 nm (Figure S6a in Supporting Information-F). The as-prepared ZnO NSs exhibit good crystallinity of the wurtzite phase (Figure S6b in the Supporting Information-F). The photocatalytic reaction rate showed that ZnO NRs are superior to ZnO NSs, ZnO NRs can achieve 29.25%, while ZnO NSs only reach 26.68% efficiency at the same time. It is observed that the photocatalytic activity of ZnO NSs tends to decelerate over an extended duration of the reaction, with the degradation rate gradually slowing down between 90 and 120 min (Figure S6c in Supporting Information-F). The degradation effect of ZnO–Ag NRs was further examined with other compounds such as phenol, which is a common pollutant found in wastewater from industrial, agricultural, and domestic activities. Remediation of phenol is challenging, and it often exhibits limited self-sensitization with visible light illumination.³⁸ The prepared ZnO–Ag NRs (1 wt %) demonstrated high photocatalytic activity for phenol degradation under white light illumination. Approximately 100% degradation of phenol was achieved after 120 min, and the characteristic absorption peak of phenol at 270 nm was completely undetectable after illumination (Figure S7a,b in Supporting Information-G).

Performance of the CNF–ZnO–Ag Membrane. The photocatalytic performance of the CNF–ZnO–Ag composite

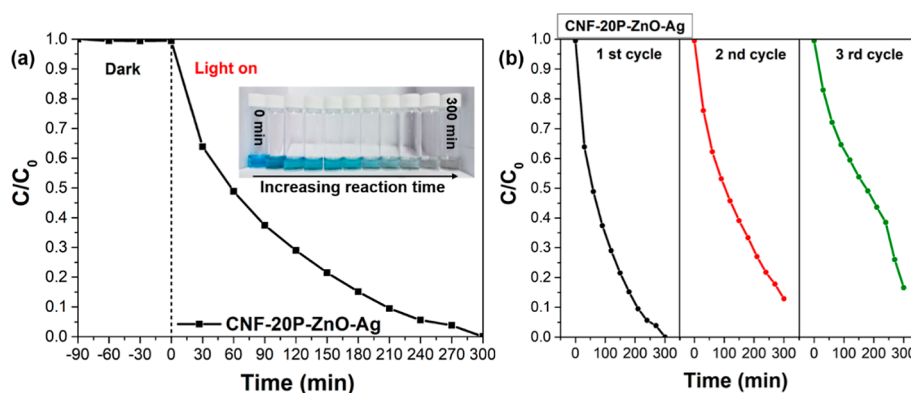


Figure 9. (a) Photocatalytic degradation rate of MB with the long time (inset of the visual image of MB solution in time of experiment) and (b) the cycling test of CNF–ZnO–Ag membrane (photograph courtesy of N. B. T. Pham. Copyright 2023).

is demonstrated in Figure 7a, where the absorption intensity of MB at 664 nm gradually decreased with increasing reaction time when immersed in the reacting solution under visible light irradiation. This observation indicates that MB was degraded as a result of the catalytic reaction of the CNF–ZnO–Ag composite. The visual degradation of the MB dye was further confirmed by the change in solution color from deep to light blue, as depicted in Figure 7b. The photocatalytic efficiency of different CNF samples under visible light is presented in Figure 7c,e. CNF alone exhibited the minimal degradation of MB, which was attributed to MB molecules adsorbing onto the CNF surface.³³ However, the significant removal efficiency of MB was observed only with the CNF decorated with ZnO–Ag NRs. After 120 min, the maximum decomposition of MB achieved was 74%, compared to 23 and 2% for CNF–ZnO and bare CNF, respectively. The photocatalytic degradation of MB over the CNF–ZnO–Ag membrane can be originated from the formation of ROS, such as $\cdot\text{O}_2^-$ and $\cdot\text{OH}$, through the photocatalytic reaction of ZnO–Ag under light irradiation. These ROS possess strong oxidizing properties and react with MB to produce carbon dioxide and water, leading to the degradation of MB.³⁹ The photocatalytic efficiency of the CNF–ZnO–Ag composite was 3.2 times higher than that of CNF–ZnO without Ag NPs. This enhancement can be attributed to the higher photogeneration of electrons in ZnO–Ag compared with ZnO. When Ag NPs are attached to the ZnO NRs, the Schottky barrier forms in the ZnO–Ag heterostructure. Upon irradiation, electrons in the valence band of ZnO move to the conduction band (CB), generating electron–hole (e^-/h^+) pairs. A schematic for the photodegradation of MB by the CNF–ZnO–Ag composite is proposed in Figure 8. The CB of ZnO is higher than the new equilibrium Fermi energy level (E_f) of ZnO–Ag, allowing for the transfer of electrons from ZnO to Ag. As a result, Ag NPs become highly enriched with electrons, reacting with oxygen and generating more superoxide radicals ($\cdot\text{O}_2^-$). Furthermore, Ag NPs exhibit LSPR properties in the visible region, allowing the excited electrons in Ag NPs to transfer the CB of ZnO NRs.⁴⁰ This renders ZnO–Ag NRs highly active in the visible region, unlike pristine ZnO that primarily responds to UV light. These effects result in reduced recombination in pristine ZnO and improved charge transfer, ultimately leading to enhanced photocatalytic efficiency of the composite.

For quantitative comparison, the degradation curves of MB were fitted using the pseudo-first-order kinetic model described by the equation $\ln(C_0/C) = kt$, where k represents

the kinetic rate constant (Figure 7d,e). The CNF membrane and the control dye showed negligible k values of 1.2×10^{-4} and $2.3 \times 10^{-4} \text{ min}^{-1}$, respectively, indicating no photodegradation activity. In contrast, the CNF–ZnO and CNF–ZnO–Ag NR decorated membranes exhibited k values of 2.2×10^{-3} and $1.1 \times 10^{-2} \text{ min}^{-1}$, respectively. Among them, the CNF–ZnO–Ag NR membrane showed the highest k value, indicating its superior photocatalytic performance. Another approach was attempted to prepare the CNF–ZnO–Ag membrane by directly synthesizing ZnO–Ag NRs onto the CNF membrane (Supporting Information–H). However, the result showed that the photodegradation efficiency of MB was not as significant as that achieved with the drop-casting method, despite using a 10-fold higher concentration of ZnO–Ag (Figure S8 in the Supporting Information–H).

Figure 9a shows the photocatalytic performance of the CNF–ZnO–Ag membrane for a longer duration compared to previous tests. The results showed that after 5 h of visible light irradiation, the CNF–ZnO–Ag membrane achieved complete removal of MB with an efficiency of 100%. The color of solution changed from a deep blue to a transparent color, confirming the complete degradation of MB using the CNF–ZnO–Ag membrane. Furthermore, to investigate the robustness of the CNF–ZnO–Ag photocatalyst composite, reusability tests were conducted by evaluating the degradation of MB (Figure 9b). The results revealed that there was no significant decrease in the photocatalytic degradation efficiency during the recycling process. After three cycles, the photocatalytic efficiency reduced by only 16.52%. This demonstrated that the CNF–ZnO–Ag composite exhibits stable photocatalytic performance for MB photodegradation under visible light irradiation. Based on these findings, it can be concluded that the CNF–ZnO–Ag membrane is a promising candidate for practical applications in the photocatalytic degradation of organic pollutants in aqueous environments. Its facile synthesis approach and excellent reusability make it a viable option for efficient and sustainable wastewater treatment.

CONCLUSIONS

In this study, we demonstrated a simple and effective approach for developing a composite membrane consisting of CNF and ZnO–Ag NRs to address the treatment of dye wastewater. CNF was utilized as the platform membrane for the composite by inducing self-entanglement through NaOH treatment, enhancing both the tensile strength and the control over the pore structure. As the photocatalyst material, ZnO–Ag NRs

were drop-dried onto the porous CNF membrane, resulting in attachment within the pores. The composite exhibited remarkable photocatalytic activity in degrading MB under visible light and displayed an excellent wet strength. The attachment between the ZnO–Ag NRs and the porous CNF structure significantly contributed to the photocatalytic performance. Furthermore, the composite demonstrated satisfactory reusability without significant deterioration after three cycles. The simple preparation method, excellent photocatalytic performance, and robustness of the composite make it a valuable solution for practical applications in the treatment of running water. Notably, when the CNF–ZnO–Ag membrane contained a minimal content of 2.20 wt % Ag nanoparticles loaded onto ZnO NRs, its photocatalytic efficiency was approximately 3.2 times higher compared to that of CNF–ZnO without Ag nanoparticles. Moreover, the CNF–ZnO–Ag membrane achieved complete decomposition of MB (10 mg L^{-1}) within 300 min, with a photocatalytic rate of $1.1 \times 10^{-2} \text{ min}^{-1}$. The utilization of CNF as a platform material provides a solution for carrying small photocatalytic particles while preventing secondary pollution. This study contributes to the development of sustainable and efficient photocatalyst composites for dye wastewater treatment.

■ ASSOCIATED CONTENT

SI Supporting Information

The Supporting Information is available free of charge at <https://pubs.acs.org/doi/10.1021/acsomega.3c09062>.

SEM images of the well-attached ZnO–Ag NRs onto CNF-10P, CNF-20P, and CNF-30P, visual images of ZnO leaked from CNF-20P in DI water, wash-out of ZnO in the CNF-20P–ZnO membrane in DI water, XRD pattern of ZnO–Ag NRs, SEM images of ZnO NRs and ZnO–Ag NRs (1 wt %), SEM image and the photocatalytic reaction rate of AgNPs, SEM image and XRD pattern of ZnO NSs, the photocatalytic reaction rate of ZnO NSs and ZnO NRs, UV absorption spectra and the photocatalytic reaction rate of phenol solution illuminated by white light for various durations in the presence of photocatalysts of ZnO–Ag NRs, and the photocatalytic reaction rate of CNF–20P–ZnO–Ag from direct synthesis (PDF)

■ AUTHOR INFORMATION

Corresponding Author

Han-Kyu Choi – Department of Chemistry, Kunsan National University, Gunsan 54150, Republic of Korea; orcid.org/0000-0003-1522-945X; Email: hchoi@kunsan.ac.kr

Authors

Jungsoo Han – Department of Bio-based Materials, Chungnam National University, Daejeon 305-764, Republic of Korea; orcid.org/0000-0002-8275-138X

Ngoc Bao Tri Pham – Department of Chemistry, Kunsan National University, Gunsan 54150, Republic of Korea

Kyudeok Oh – Department of Agriculture, Forestry and Bioresources Program in Environmental Materials Science, College of Agriculture and Life Sciences, Seoul National University, Seoul 08826, Republic of Korea

Complete contact information is available at: <https://pubs.acs.org/doi/10.1021/acsomega.3c09062>

Author Contributions

J.H. and N.B.T.P. are the cofirst authors. J.H.: Conceptualization and writing—original draft and data acquisition. N.B.T.P.: Conceptualization, writing—original draft, and data acquisition. K.O.: Writing—review and editing. H.-K.C.: Conceptualization and writing—review and editing.

Notes

The authors declare no competing financial interest.

■ ACKNOWLEDGMENTS

This research was supported by the “Regional Innovation Strategy” through the National Research Foundation of Korea (NRF) funded by the Ministry of Education (2023RIS-008).

■ REFERENCES

- (1) Ren, G.; Han, H.; Wang, Y.; Liu, S.; Zhao, J.; Meng, X.; Li, Z. Recent Advances of Photocatalytic Application in Water Treatment: A Review. *Nanomaterials* **2021**, *11*, 1804.
- (2) Kulis-Kapuscinska, A.; Kwoka, M.; Borysiewicz, M. A.; Wojciechowski, T.; Licciardello, N.; Sgarzi, M.; Cuniberti, G. Photocatalytic degradation of methylene blue at nanostructured ZnO thin films. *Nanotechnol* **2023**, *34*, 155702.
- (3) Gaur, J.; Vikrant, K.; Kim, K.-H.; Kumar, S.; Pal, M.; Badru, R.; Masand, S.; Momoh, J. Photocatalytic degradation of Congo red dye using zinc oxide nanoparticles prepared using Carica papaya leaf extract. *Mater. Today Sustain* **2023**, *22*, 100339.
- (4) Alzahrani, H. A. H.; Almulaiky, Y. Q.; Alsaiani, A. O. The photocatalytic dye degradation of methylene blue (MB) by nanostructured ZnO under UV irradiation. *Phys. Scr.* **2023**, *98*, 045703.
- (5) Wojtasik, K.; Zięba, M.; Tyszkiewicz, C.; Pakiel, W.; Żak, G.; Jeremiasz, O.; Gondek, E.; Drabczyk, K.; Karasiński, P. Zinc Oxide Films Fabricated via Sol-Gel Method and Dip-Coating Technique—Effect of Sol Aging on Optical Properties, Morphology and Photocatalytic Activity. *Mater.* **2023**, *16*, 1898.
- (6) Lee, K. M.; Lai, C. W.; Ngai, K. S.; Juan, J. C. Recent developments of zinc oxide based photocatalyst in water treatment technology: A review. *Water Res.* **2016**, *88*, 428–448.
- (7) Ha, L. P. P.; Vinh, T. H. T.; Thuy, N. T. B.; Thi, C. M.; Viet, P. V. Visible-light-driven photocatalysis of anisotropic silver nanoparticles decorated on ZnO nanorods: Synthesis and characterizations. *J. Environ. Chem. Eng.* **2021**, *9*, 105103.
- (8) Hu, J.; You, N.; Yu, Z.; Zhou, G.; Xu, X. Two-dimensional ZnO ultrathin nanosheets decorated with Au nanoparticles for effective photocatalysis. *J. Appl. Phys.* **2016**, *120*, 074301.
- (9) Al-Gharibi, M. A.; Kyaw, H. H.; Al-Sabahi, J. N.; Myint, M. T. Z.; Al-Sharji, Z. A.; Al-Abri, M. Z. Silver nanoparticles decorated zinc oxide nanorods supported catalyst for photocatalytic degradation of paracetamol. *Mater. Sci. Semicond* **2021**, *134*, 105994.
- (10) Sanzone, G.; Zimbone, M.; Cacciato, G.; Ruffino, F.; Carles, R.; Privitera, V.; Grimaldi, M. G. Ag/TiO₂ nanocomposite for visible light-driven photocatalysis. *Superlattices Microstruct.* **2018**, *123*, 394–402.
- (11) Guo, Y.; Fu, X.; Liu, R.; Chu, M.; Tian, W. Efficient green photocatalyst of Ag/ZnO nanoparticles for methylene blue photodegradation. *J. Mater. Sci.: Mater. Electron.* **2022**, *33*, 2716–2728.
- (12) Ahmad, M.; Qureshi, M. T.; Rehman, W.; Alotaibi, N. H.; Gul, A.; Abdel Hameed, R. S.; Elaimi, M. A.; Abd el-kader, M. F. H.; Nawaz, M.; Ullah, R. Enhanced photocatalytic degradation of RhB dye from aqueous solution by biogenic catalyst Ag@ZnO. *J. Alloys Compd.* **2022**, *895*, 162636.
- (13) Gupta, G. K.; Mondal, M. K. Fundamentals and mechanistic pathways of dye degradation using photocatalysts. In *Photocatalytic Degradation of Dyes Current Trends and Future Perspectives*; Shah, M., Dave, S., Das, J., Eds.; Elsevier Inc Amsterdam, 2021, pp 527–545.
- (14) Nechyporchuk, O.; Belgacem, M. N.; Bras, J. Production of cellulose nanofibrils: A review of recent advances. *Ind. Crops Prod.* **2016**, *93*, 2–25.

- (15) Han, J. S.; Kim, S. Y.; Seo, Y. B. Development of quality evaluation method for cellulose fibrils. *Cellulose* **2022**, *29*, 6549–6563.
- (16) Tian, C.; Luo, S.; She, J.; Qing, Y.; Yan, N.; Wu, Y.; Liu, Z. Cellulose nanofibrils enable flower-like BiOCl for high-performance photocatalysis under visible-light irradiation. *Appl. Surf. Sci.* **2019**, *464*, 606–615.
- (17) Dehghani, M.; Nadeem, H.; Raghuvanshi, V. S.; Mahdavi, H.; Banaszak Holl, M. M.; Batchelor, W. ZnO/Cellulose Nanofiber Composites for Sustainable Sunlight-Driven Dye Degradation. *ACS Appl. Nano Mater.* **2020**, *3*, 10284–10295.
- (18) Shi, C.; Zhang, L.; Bian, H.; Shi, Z.; Ma, J.; Wang, Z. Construction of Ag-ZnO/cellulose nanocomposites via tunable cellulose size for improving photocatalytic performance. *J. Clean. Prod.* **2021**, *288*, 125089.
- (19) Dehghani, M.; Naseri, M.; Nadeem, H.; Banaszak Holl, M. M.; Batchelor, W. Sunlight-driven photocatalytic per- and polyfluoroalkyl substances degradation over zinc oxide/cellulose nanofiber catalyst using a continuous flow reactor. *J. Environ. Chem. Eng.* **2022**, *10*, 108686.
- (20) Dadigala, R.; Bandi, R.; Alle, M.; Park, C.-W.; Han, S.-Y.; Kwon, G.-J.; Lee, S.-H. Effective fabrication of cellulose nanofibrils supported Pd nanoparticles as a novel nanozyme with peroxidase and oxidase-like activities for efficient dye degradation. *J. Hazard. Mater.* **2022**, *436*, 129165.
- (21) Wei, Y.; Wang, X.; Yi, G.; Zhou, L.; Cao, J.; Sun, G.; Chen, Z.; Bala, H.; Zhang, Z. Hydrothermal synthesis of Ag modified ZnO nanorods and their enhanced ethanol-sensing properties. *Mater. Sci. Semicond. Process.* **2018**, *75*, 327–333.
- (22) Forsberg, D. C. R.; Westin, P.-O.; Li, L.; Svedberg, A.; Grundberg, H.; Berglund, L. A. A method for chemical and physical modification of oriented pulp fibre sheets. *Cellulose* **2022**, *29*, 8371–8386.
- (23) Abe, K.; Yano, H. Formation of hydrogels from cellulose nanofibers. *Carbohydr. Polym.* **2011**, *85*, 733–737.
- (24) Henriksson, G.; Lennholm, H. Cellulose and Carbohydrate Chemistry. In *Pulp and Paper Chemistry and Technology*; Monika, E. K., Gellerstedt, G., Henriksson, G., Eds.; Wood Chemistry and Wood Biotechnology de Gruyter: Berlin, 2009; Vol. 1, pp 72–99.
- (25) Sawada, D.; Nishiyama, Y.; Shah, R.; Forsyth, V. T.; Mossou, E.; O'Neill, H. M.; Wada, M.; Langan, P. Untangling the threads of cellulose mercerization. *Nat. Commun.* **2022**, *13*, 6189.
- (26) Nakano, T.; Tanimoto, T.; Hashimoto, T. Morphological change induced with NaOH-water solution for ramie fiber: change mechanism and effects of concentration and temperature. *J. Mater. Sci.* **2013**, *48*, 7510–7517.
- (27) Nakano, T. Modeling of the morphological change of cellulose microfibrils caused with aqueous NaOH solution: the longitudinal contraction and laterally swelling during decrystallization. *J. Mol. Model.* **2017**, *23*, 129.
- (28) Marzouki, R.; Brahmia, A.; Bondock, S.; Keshk, S.; Zid, M. F.; Al-Sehemi, A. G.; Koschella, A.; Heinze, T. Mercerization effect on structure and electrical properties of cellulose: Development of a novel fast Na-ionic conductor. *Carbohydr. Polym.* **2019**, *221*, 29–36.
- (29) Bairagi, S.; Banerjee, S.; Chowdhury, A.; Ali, S. W. Development of a Sustainable and Flexible Piezoelectric-cum-Triboelectric Energy Harvester Comprising a Simple Commodity Cotton Fabric. *ACS Sustain. Chem. Eng.* **2021**, *9*, 4004–4013.
- (30) Abebe, B.; Murthy, H. A.; Amare, E. Enhancing the photocatalytic efficiency of ZnO: Defects, heterojunction, and optimization. *Environ. Nanotechnol.* **2020**, *14*, 100336.
- (31) Liu, T.; Lu, Z.; Zhai, H.; Meng, J.; Song, J.; Zhang, Y.; Liu, J.; Li, J. Hierarchical Porous PLLA@TiO₂ Fibrous Membrane for Enhanced and Stable Photocatalytic Degradation Efficiency. *ACS ES&T Water* **2023**, *3*, 342–353.
- (32) Elbakry, S.; Ali, M. E. A.; Abouelfadl, M.; Badway, N. A.; Salam, K. M. M. Photocatalytic degradation of organic compounds by TFC membranes functionalized with Ag/rGO nanocomposites. *J. Photochem. Photobiol., A* **2022**, *430*, 113957.
- (33) Chen, Y.; Xiang, Z.; Wang, D.; Kang, J.; Qi, H. Effective photocatalytic degradation and physical adsorption of methylene blue using cellulose/GO/TiO₂ hydrogels. *RSC Adv.* **2020**, *10*, 23936–23943.
- (34) Ma, J.; Zhu, W.; Tian, Y.; Wang, Z. Preparation of Zinc Oxide-Starch Nanocomposite and Its Application on Coating. *Nanoscale Res. Lett.* **2016**, *11*, 200.
- (35) Bazant, P.; Kuritka, I.; Munster, L.; Kalina, L. Microwave solvothermal decoration of the cellulose surface by nanostructured hybrid Ag/ZnO particles: a joint XPS, XRD and SEM study. *Cellulose* **2015**, *22*, 1275–1293.
- (36) Kavitha, S. R.; Umadevi, M.; Janani, S. R.; Balakrishnan, T.; Ramanibai, R. Fluorescence quenching and photocatalytic degradation of textile dyeing waste water by silver nanoparticles. *Spectrochim. Acta, Part A* **2014**, *127*, 115–121.
- (37) Balamurugan, V.; Muruganandam, L.; Natarajan, R. Photocatalytic activity of silver nanoparticles synthesized using cadiospermum halicacabum and moringa oleifera leaf extract. *Mater. Today: Proc.* **2022**, *62*, 5365–5370.
- (38) Vo, N. T. T.; You, S.-J.; Pham, M.-T.; Pham, V. V. A green synthesis approach of p-n CuO/ZnO junctions for multifunctional photocatalysis towards the degradation of contaminants. *Environ. Technol. Innovation* **2023**, *32*, 103285.
- (39) Li, B.; Kim, I. S.; Dai, S.; Sarwar, M. N.; Yang, X. Heterogeneous Ag@ZnO nanorods decorated on polyacrylonitrile fiber membrane for enhancing the photocatalytic and antibacterial properties. *Colloids Interface Sci. Commun.* **2021**, *45*, 100543.
- (40) Mahardika, T.; Putri, N. A.; Putri, A. E.; Fauzia, V.; Roza, L.; Sugihartono, I.; Herbani, Y. Rapid and low temperature synthesis of Ag nanoparticles on the ZnO nanorods for photocatalytic activity improvement. *Results Phys.* **2019**, *13*, 102209.